Inorganic Chemistry
Article
Cite This: Inorg. Chem. XXXX, XXX, XXX−XXX
pubs.acs.org/IC

Zirconium Metal−Organic Frameworks Assembled from Pd and Pt P^NN^NP Pincer Complexes: Synthesis, Postsynthetic Modification, and Lewis Acid Catalysis

Benjamin R. Reiner, Neil T. Mucha, Anna Rothstein, J. Sebastian Temme, Pu Duan, Klaus Schmidt-Rohr, Bruce M. Foxman, and Casey R. Wade*,†,‡

†Department of Chemistry, Brandeis University, 415 South Street MS 015, Waltham, Massachusetts 02453, United States

Supporting Information

ABSTRACT: Carboxylic acid-functionalized Pd and Pt P^NN^NP pincer complexes were used for the assembly of two porous Zr metal−organic frameworks (MOFs), 2-PdX and 2-PtX. Powder X-ray diffraction analysis shows that the new MOFs adopt cubic framework structures similar to the previously reported $Zr_6O_4(OH)_4[(P^OC^OP)PdX]_3$, [$P^OC^OP$ = 2,6-$(OPAr_2)_2C_6H_3$); Ar = p-$C_6H_4CO_2^-$, X = Cl^-, I^-] (1-PdX). Elemental analysis and spectroscopic characterization indicate the presence of missing linker defects, and 2-PdX and 2-PtX were formulated as $Zr_6O_4(OH)_4(OAc)_{2.4}[M(P^NN^NP)X]_{2.4}$ [M = Pd, Pt; P^NN^NP = 2,6-$(HNPAr_2)_2C_5H_3N$; Ar = p-$C_6H_4CO_2^-$; X = Cl^-, I^-]. Postsynthetic halide ligand exchange reactions were carried out by treating 2-PdX with $Ag(O_3SCF_3)$ or NaI followed by $PhI(O_2CCF_3)_2$. The latter strategy proved to be more effective at activating the MOF for the catalytic intramolecular hydroamination of an o-substituted alkynyl aniline, underscoring the advantage of using halide exchange reagents that produce soluble byproducts.

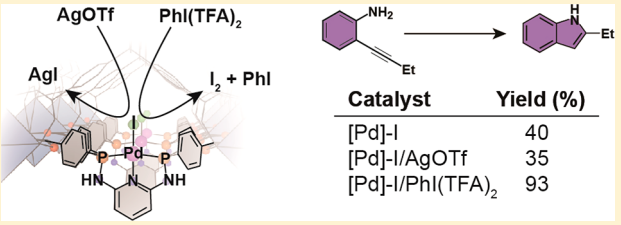

INTRODUCTION

Transition-metal complexes supported by arene-based diphosphine pincer ligands (P^ZE^ZP, Figure 1) have been found to

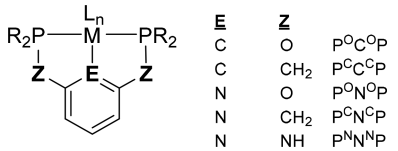

E	Z	
C	O	P^OC^OP
C	CH_2	P^CC^CP
N	O	P^ON^OP
N	CH_2	P^CN^CP
N	NH	P^NN^NP

Figure 1. General structure of P^ZE^ZP pincer complexes.

catalyze a wide range of organic transformations and small molecule activation reactions.[1−21] Much of the appeal and success of P^ZE^ZP pincer ligand platforms arises from their tunability and the stability conferred by chelation. We and others have been interested in incorporating transition-metal P^ZE^ZP complexes into porous metal−organic frameworks (MOFs).[22−25] In addition to offering ease of product separation and recyclability, heterogenization of homogeneous catalysts can potentially improve catalyst lifetime and activity via site isolation or other immobilization effects. MOFs have attracted considerable interest as heterogeneous catalyst platforms owing to their well-defined structures, inherent porosity, and amenability to functionalization.[26−32]

We recently reported the synthesis and characterization of a Zr MOF, 1-PdX, assembled from a linker based on a Pd P^OC^OP pincer complex (Scheme 1).[22] The MOF exhibits markedly better catalytic activity for transfer hydrogenation of aldehydes

Scheme 1. Synthesis and Framework Structure of 1-PdX

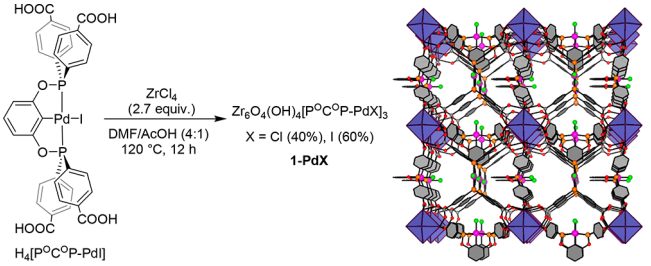

than an analogous homogeneous Pd P^OC^OP complex, and the difference in activity was attributed to inhibition of catalyst decomposition pathways in the MOF. Humphrey and coworkers employed a similar design strategy to prepare a Co MOF containing Pd P^CC^CP linkers and showed that the material activates CO_2 under mild conditions after Cl^-/CH_3^- ligand exchange at the Pd pincer sites.[23] Stoddart, Farha, and coworkers used solvent-assisted ligand incorporation to immobilize Ir P^OC^OP complexes within the mesoporous Zr MOF NU-1000, and the resulting material was found to catalyze the gas phase hydrogenation of ethylene.[24]

Although the identities of the central arene donor (E) and phosphine linker groups (Z) can have a profound impact on reactivity, P^ZE^ZP pincer complexes often exhibit similar

Received: December 4, 2017

DOI: 10.1021/acs.inorgchem.7b03063
Inorg. Chem. XXXX, XXX, XXX−XXX

molecular structures.[9,33−35] This led us to consider that an isostructural series of MOFs might be obtained using P^ZE^ZP pincer metallolinkers with different arene donors, linker groups, or even chelated metal species. To explore this possibility and the scope of immobilization and site isolation effects, we have been investigating the assembly of Zr MOFs from linkers based on P^NN^NP pincer complexes. Herein, we report the synthesis and characterization of two porous Zr MOFs, 2-PdX and 2-PtX, constructed from Pd and Pt P^NN^NP pincer complexes. These materials adopt the same cubic framework structure as 1-PdX, providing initial evidence that the isoreticular principle can be applied to pincer MOFs. In addition, postsynthetic halide ligand exchange reactions at the Pd centers of 2-PdX were investigated as a means of activating the MOF for Lewis acid-catalyzed transformations. Silver salts are ubiquitous and operationally simple halide abstraction agents, but precipitation of insoluble AgX salts can potentially pollute a heterogeneous catalyst. As a result, halide abstraction becomes uniquely challenging in MOFs owing to the need for soluble byproducts that can be easily separated from the heterogeneous catalyst. We previously reported the use of $PhI(TFA)_2$ (TFA = O_2CCF_3) for I^-/TFA^- ligand exchange in 1-PdX and considered this reagent to be advantageous because it produces PhI and I_2 as soluble byproducts.[22] Herein, we further highlight the efficacy of this strategy, demonstrating that Cl^-/I^- ligand exchange in 2-PdX followed by reaction with $PhITFA_2$ is superior to treatment with AgOTf (OTf = O_3SCF_3) for activating the MOF as a Lewis acid catalyst for intramolecular hydroamination.

RESULTS AND DISCUSSION

Synthesis and Characterization of 2-PdX and 2-PtX. The ligand ^{t}Bu$_4$L was prepared by the P−N coupling of $ClP(C_6H_4CO_2{}^tBu)_2$ with 2,6-diaminopyridine in the presence of triethylamine (Scheme 2).[36] The M−Cl pincer complexes, ^{t}Bu$_4$L-MCl (M = Pd, Pt), were obtained by reaction of ^{t}Bu$_4$L with an equimolar amount of the appropriate MCl_2(cod) (cod = 1,5-cyclooctadiene) metal precursor in CH_2Cl_2 solution. Subsequent Cl^-/I^- exchange with NaI generated the pincer complexes ^{t}Bu$_4$L-PdI and ^{t}Bu$_4$L-PtI. The $^{31}P\{^1H\}$ NMR spectra of the ^{t}Bu$_4$L-MX (X = Cl, I) complexes exhibit a single resonance in the 61−76 ppm range with the signals for the ^{t}Bu$_4$L-MI complexes shifted slightly downfield relative to the chloride analogues (Figures S9, S12, S18, S21). The ^1H NMR spectra of these complexes display all expected resonances.

Scheme 2. Synthesis of Pincer Complexes H_3L-MI.[a]

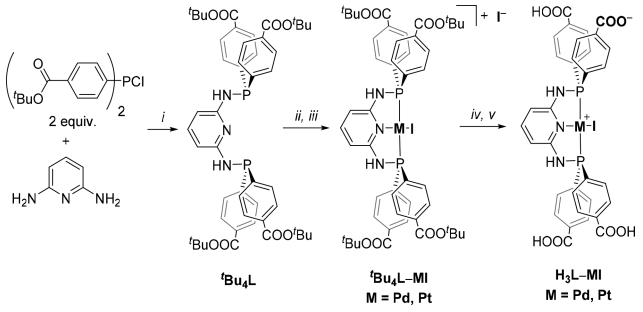

[a]Conditions: (i) NEt_3, toluene, 80 °C, 16 h; (ii) MCl_2(cod), CH_2Cl_2, 16 h; (iii) NaI, acetone, 1.5 h; (iv) CF_3CO_2H, CH_2Cl_2, 16 h; (v) pyridine, acetone, 0.5 h

^{t}Bu$_4$L-PdI and ^{t}Bu$_4$L-PtI were deprotected by reaction with trifluoroacetic acid (HTFA) in CH_2Cl_2 solution. The crude products were then treated with pyridine (1.5 equiv) in acetone solution, resulting in elimination of 1 equiv of HI and isolation of the zwitterionic complexes H_3L-MI. The $^{31}P\{^1H\}$ NMR spectra of the H_3L-MI complexes exhibit broadened resonances centered at 69.9 and 63.2 ppm for M = Pd and Pt, respectively (Figures S15 and S24). Single crystals of H_3L-PdI were obtained from a saturated methanol solution, and the X-ray crystal structure supports deprotonation of one of the carboxylate groups concomitant with loss of the outer sphere I^- to form the zwitterionic complex (Figure S1).

Solvothermal reaction of the H_3L-MI (M = Pd, Pt) complexes with $ZrCl_4$ in a 4/1 v/v mixture of *N*,*N*-dimethylformamide (DMF) and acetic acid (AcOH) generates 2-PdX and 2-PtX as bright yellow and white microcrystalline powders, respectively (Scheme 3). Notably, attempts to use the deprotected chloride derivatives (i.e., H_3L-MCl) for MOF synthesis resulted only in the formation of dark, amorphous solids. A similar trend was previously observed for the synthesis of Zr MOFs from H_4[POCOP-PdX] (X = Cl, I) complexes.[22] The contrasting behavior of the M−Cl and M−I complexes likely reflects the difference in leaving group ability between Cl^- and I^- ligands.[37] The more strongly bound I^- ligands ostensibly act as protecting groups, suppressing ligand exchange and subsequent decomposition processes under the solvothermal reaction conditions.

Scheme 3. Synthesis of 2-PdX and 2-PtX

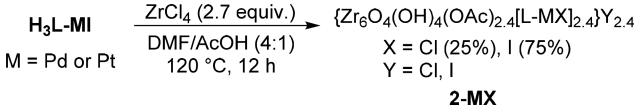

The powder X-ray diffraction (PXRD) data show that 2-PdX and 2-PtX are isostructural with 1-PdX (Figure 2). Full-pattern decomposition of the data was performed using Pawley refinement and provided cubic unit cell parameters of a = 16.76 and 16.81 Å for 2-PdX and 2-PtX, respectively (Tables S2 and S3 and Figures S2 and S3). 2-PdX and 2-PtX are both stable under ambient conditions but experience loss of crystallinity upon methanol solvent exchange followed by drying in vacuo. Optimized workup conditions include washing with DMF and acetone followed by soaking (ca. 16 h) in acetone prior to drying under reduced pressure. Following this procedure, samples of 2-PdX and 2-PtX were desolvated by heating under reduced pressure (10^{-4} Torr) at 150 °C for 16 h. N_2 adsorption measurements (77 K) (Figure S4) gave calculated Brunauer−Emmett−Teller (BET) surface areas of 922 and 726 $m^2\ g^{-1}$ for 2-PdX and 2-PtX, respectively, which are comparable to that previously observed for 1-PdX (1164 $m^2\ g^{-1}$). Pore size distribution analyses for 1-PdX, 2-PdX, and 2-PtX using the DFT method show similar major pore distributions around 10−12 Å that are consistent with the proposed structure (Figure S5). However, 2-PdX and 2-PtX exhibit a broad distribution of larger pores in the 14−20 Å range that could be attributable to the presence of missing linker defects.

Combustion analysis and inductively coupled plasma optical emission spectrometry (ICP-OES) were used to determine the

DOI: 10.1021/acs.inorgchem.7b03063
Inorg. Chem. XXXX, XXX, XXX−XXX

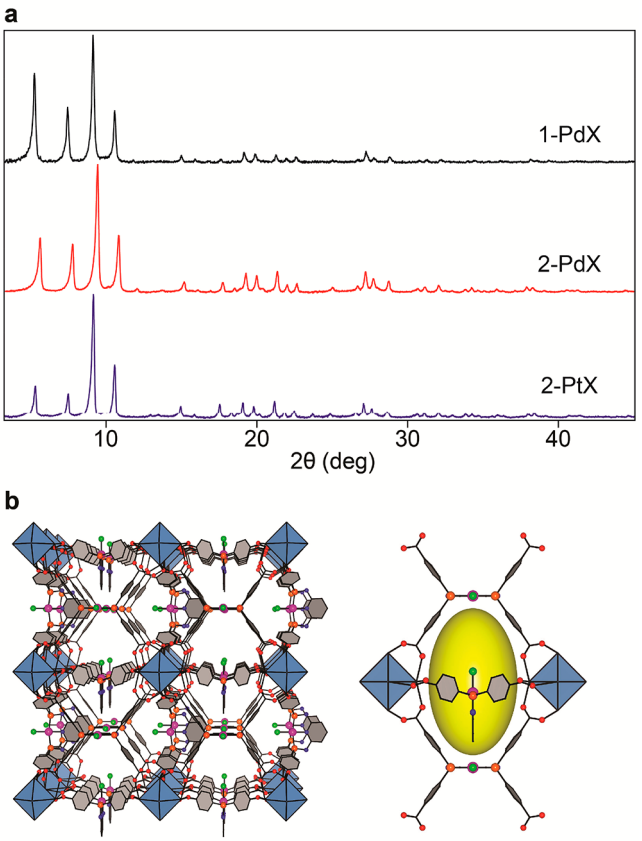

Figure 2. (a) PXRD patterns of 1-PdX, 2-PdX, and 2-PtX (Cu Kα radiation, λ = 1.54 Å). (b) Defect-free framework structure of 2-MX. (c) View of a portion of the framework showing ovoidal pores. Blue octahedra represent $[Zr_6O_4(OH)_4]^{12+}$ building units.

compositions of desolvated samples of 2-PdX and 2-PtX. ICP-OES provided Zr:M (M = Pd, Pt) ratios of 2.9:1 and 2.7:1 for 2-PdX and 2-PtX, respectively. These values reflect deficiencies of Pd and Pt based on the formula expected from the framework structure $(Zr_6O_4(OH)_4[MX(P^NN^NP)X]_3)$ and are likely the result of missing linker-type defects (vide infra).[38−46] The elemental analysis data provide M:I:Cl molar ratios of 1:0.82:0.88 and 1:0.66:0.74 for 2-PdX and 2-PtX, respectively, indicating that a significant amount of Cl^- is introduced from the use of $ZrCl_4$ for the MOF synthesis. An overall 1:2 M:halide ratio is expected if the halides provide charge balance of the cationic pincer complexes. Consequently, the experimentally determined ratios reflect the partial absence of charge balancing outer sphere halides. We have not clearly identified the remaining charge-balancing species, but it is possible that acetate or deprotonated Zr_6 SBUs may fulfill this role.[47]

2-PdX and 2-PtX were characterized by solid and solution state NMR spectroscopy as well as electrospray mass spectrometry (ESI-MS) to gain further insight into their structure and composition. The solid-state ^{31}P NMR spectra of 2-PdX and 2-PtX show broad, asymmetric signals centered at 72 and 67 ppm, respectively (Figure 3). The spectra also show the presence of a minor species, giving rise to a signal around 25 ppm. The chemical shift of the minor species is in line with that observed for the P^NN^NP pincer ligand in solution but could also arise from a small amount of ligand decomposition.[22] Although ligand decomposition is likely to result in the presence of oxidized phosphine species, no P═O stretching

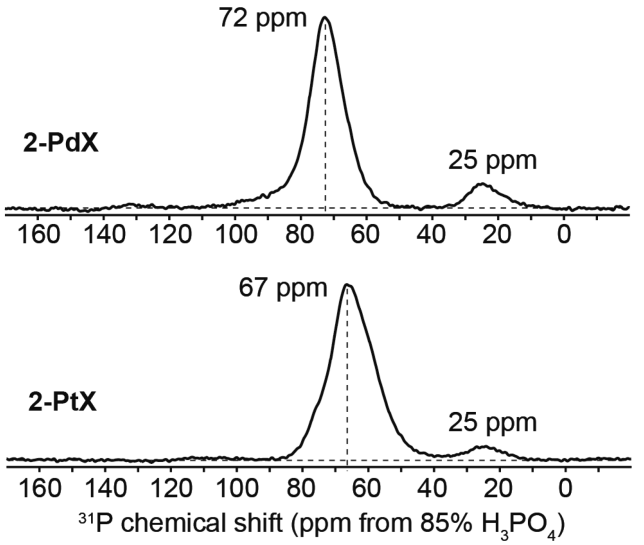

Figure 3. Solid-state ^{31}P NMR spectra of 2-PdX and 2-PtX with magic-angle spinning (MAS) and total suppression of spinning sidebands (TOSS).[48] See Supporting Information for experimental details.

bands could be clearly identified in the ATR−IR spectra of 2-PdX and 2-PtX (Figure S52).

Samples of 2-PdX and 2-PtX were digested with a 3:1 v:v mixture of trifluoroacetic acid (HTFA) and C_6D_6, and the resulting solutions were analyzed by ^{31}P and ^1H NMR spectroscopy and ESI-MS. The $^{31}P\{^1H\}$ NMR spectra each exhibit two major signals appearing at 74.0 and 69.9 ppm for 2-PdX and 67.7 ($^1J_{195Pt-P}$ = 1359.1 Hz) and 64.0 ($^1J_{195Pt-P}$ = 1394.4 Hz) ppm for 2-PtX (Figure 4). In both cases, the signals

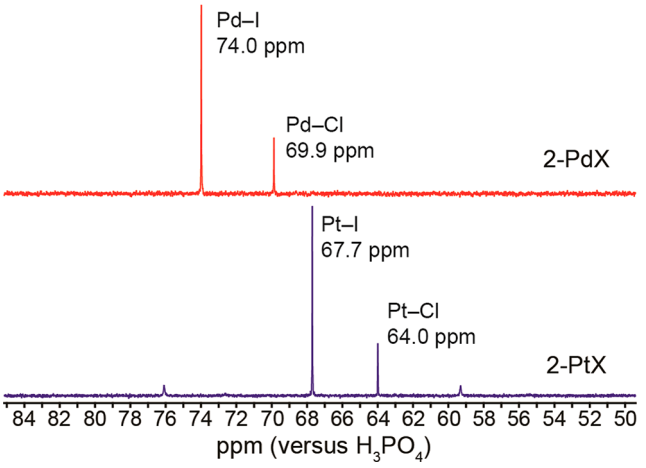

Figure 4. $^{31}P\{^1H\}$ NMR spectra of acid digested samples of 2-PdX (top) and 2-PtX (bottom).

appear in ~3:1 ratio, which was reproducible over several samples. The ^1H NMR spectra of the digested samples also clearly show two sets of resonances consistent with the presence of two distinct pincer complexes (Figures S28 and S30). The solid and solution state NMR data for the MOFs closely resemble those obtained for the H_3L-MCl and H_3L-MI complexes in solution, indicating that the pincer complex linkers remain intact both within the MOF and in solution after acid digestion. ESI-MS analysis confirmed the identity of the species present in the digested solution as the M−I and M−Cl

DOI: 10.1021/acs.inorgchem.7b03063
Inorg. Chem. XXXX, XXX, XXX−XXX

pincer complexes. The mass spectrum of 2-PdX shows two major parent ions with m/z = 795 and 886 amu that are assigned to H_4[L-PdCl]$^+$ and H_4[L-PdI]$^+$, respectively (Figure S39). Similarly, H_4[L-PtCl]$^+$ (m/z = 883 amu) and H_4[L-PtI]$^+$ (m/z = 975 amu) were observed to be the major parent ions present in the mass spectrum of 2-PtX (Figure S40). Together, these data support mixed occupancy of the M-coordinated halide.

In addition to the resonances assigned to the pincer complexes, the ^{1}H NMR spectra of digested samples of 2-PdX and 2-PtX display signals attributable to acetic acid (HOAc) at 1.86 ppm (Figures S28 and S30). Because desolvated samples were used for digestion, HOAc is not likely to be present as a pore-occluding guest molecule but rather incorporated into the framework structure as OAc$^-$. Assignment of framework bound acetate is further supported by quantitative solid-state ^{13}C NMR spectra of 2-PdX and 2-PtX that show signals consistent with acetate groups at 22 and 179 ppm (Figure S37). The CH_3 resonances at 22 ppm exhibit significant line broadening and partial dipolar dephasing that is in contrast to the sharp signal of a highly mobile species, assigned to residual acetone, at 30 ppm. These characteristics confirm the solid-like behavior of the OAc$^-$ species in the MOF. Integration of the solution-state ^{1}H and solid-state ^{13}C NMR spectra provides H_4[L-MX]$^+$:OAc ratios of ~1:1 for both MOF samples. These data combined with the Zr:M ratios determined by ICP-OES analysis suggest that the empirical formulas of 2-PdX and 2-PtX are best given as $\{Zr_6O_4(OH)_4(OAc)_{2.4}[L\text{-}MX]_{2.4}\}Y_{2.4}$. The presence of OAc$^-$ or other modulator-derived anions often signals the presence of missing linker defects in Zr MOFs.[38−42] It seems likely that 2-PdX and 2-PtX retain the same framework structure as 1-PdX but contain a larger number of disordered missing linker defects. However, given the level of uncertainty associated with structure determination from powder X-ray diffraction data, we cannot rule out the possibility of alternate framework structures. Efforts to obtain samples suitable for single crystal X-ray diffraction have not yet been successful.

Postsynthetic Halide Ligand Exchange. Exchange of halide ligands for more weakly coordinating anions is often necessary to activate homogeneous organometallic complexes for catalysis. We previously observed that treatment of 1-PdX with PhI(TFA)$_2$ facilitates I$^-$/TFA$^-$ ligand exchange, activating the MOF for transfer hydrogenation catalysis.[22] This halide exchange strategy is advantageous because it produces PhI and I_2 as soluble byproducts that can be easily separated from the MOF. Consequently, we sought to determine if a similar approach could be used for halide ligand exchange in 2-PdX.

In our initial screening, 2-PdX was treated with a solution of PhI(TFA)$_2$ in MeCN and washed copiously with MeCN (Scheme 4). ^{31}P{^{1}H} NMR analysis of the acid-digested product indicated that the H_4[L-PdCl]$^+$ pincer complex was the major species in solution (Figure 5). This result is consistent with oxidative exchange of I$^-$ for TFA$^-$ followed by coordination of the outer sphere Cl$^-$ ions that remain present in 2-PdX. To circumvent the formation of Pd−Cl species, we subjected 2-PdX to a Cl$^-$/I$^-$ ligand exchange reaction prior to treatment with PhI(TFA)$_2$. Accordingly, 2-PdI was generated by treating 2-PdX with an aqueous solution of NaI. The ^{31}P{^{1}H} NMR spectrum of an acid-digested sample of 2-PdI exhibits a single major resonance at 74.0 ppm, and the ^{1}H NMR spectrum displays a single set of well-resolved signals (Figure S32). The spectra match those expected for the Pd−I

Scheme 4. Postsynthetic Halide Ligand Exchange Reactions of 2-PdX

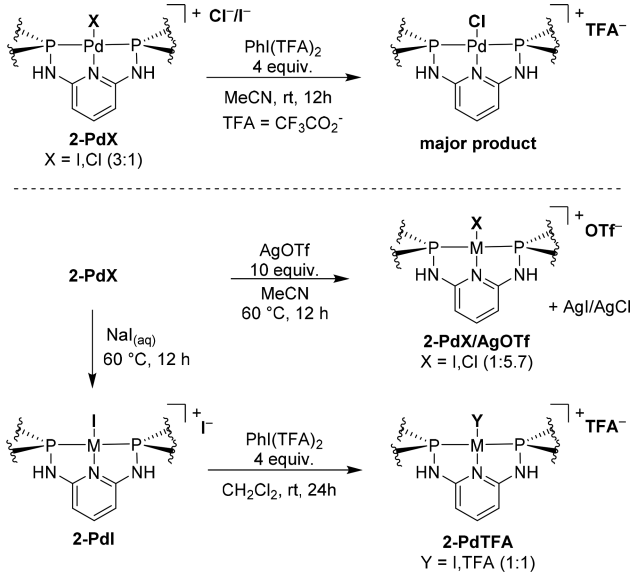

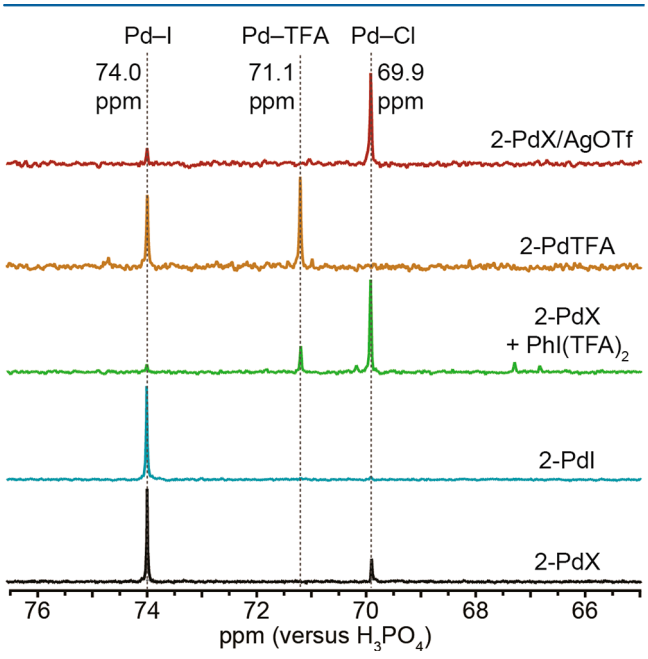

Figure 5. ^{31}P{^{1}H} NMR spectra of digested samples of 2-PdX, 2-PdI, 2-PdX + PhI(TFA)$_2$, 2-PdTFA, and 2-PdOTf/AgOTf.

pincer complex and indicate quantitative Cl$^-$/I$^-$ exchange. Moreover, the ESI-MS spectrum of the digested product contains a major signal corresponding to the H_4[L-PdI]$^+$ parent ion at m/z = 886 (Figure S41). Next, 2-PdI was treated with a CH_2Cl_2 solution of PhI(TFA)$_2$ (4 equiv per Pd), and after 24 h, the supernatant solution had turned a pink color, signaling the formation of I_2. The ^{31}P{^{1}H} NMR spectrum of an acid-digested sample of the resulting material, 2-PdTFA, features two singlets centered at 74.0 and 71.1 ppm that appear in a ~1:1 ratio. The downfield signal is consistent with the presence of unreacted H_4[L-PdI]$^+$ species, while the chemical shift of the new resonance at 71.1 ppm closely matches that observed for the analogous homogeneous complex, ^{t}Bu$_4$L-PdTFA, in the same solvent mixture (Figure S43). Consequently, the data indicate ~50% conversion of the Pd−I sites to Pd−TFA.

DOI: 10.1021/acs.inorgchem.7b03063
Inorg. Chem. XXXX, XXX, XXX−XXX

Efforts to increase conversion by resubjecting the product to $PhI(TFA)_2/CH_2Cl_2$ solutions were largely unsuccessful. After the second treatment, only a faint color change was observed for the reaction supernatant, and ^{31}P NMR analysis showed no significant changes in the Pd−I:Pd−TFA product ratio (Figure S44).

The precipitation of highly insoluble AgX byproducts makes silver-based reagents convenient for halide abstraction reactions involving soluble organometallic complexes. However, these reagents are potentially problematic for use with MOFs because the solid AgX cannot be easily separated. Considering the ubiquity of silver-based precatalyst activation, we wanted to investigate the effectiveness of silver salts for halide exchange in 2-PdX. A suspension of 2-PdX in MeCN was treated with AgOTf ($OTf^- = O_3SCF_3^-$) and heated at 60 °C for 12 h to generate 2-PdX/AgOTf. PXRD analysis confirms that 2-PdX/AgOTf retains crystallinity after the reaction. However, the pattern also contains peaks corresponding to crystalline AgCl and AgI (Figure 6), and these byproducts could not be removed by washing with common organic solvents. The $^{31}P\{^1H\}$ NMR spectrum of an acid-digested sample of 2-PdX/AgOTf ($CF_3CO_2H:C_6D_6$, 3:1 v:v) exhibits two major resonances at 69.9 and 74.0 ppm (Figure 5). These resonances closely resemble those expected for the Pd−Cl and Pd−I species, albeit appearing in a different ratio (Pd−Cl:Pd−I ≈ 5.7:1) than was observed for 2-PdX (~1:3). The homogeneous complex ^{t}Bu$_4$L-PdOTf was prepared by reaction of tBu$_4$L-PdCl with AgOTf in MeCN solution and observed to give rise to a $^{31}P\{^1H\}$ NMR signal at 75.5 ppm in the $CF_3CO_2H:C_6D_6$ solvent mixture (Figure S42). Thus, the $^{31}P\{^1H\}$ NMR spectrum of the digested sample of 2-PdX/AgOTf does not reflect the presence of Pd−OTf species in solution. Nevertheless, the appearance of crystalline AgI and AgCl in the PXRD patterns of 2-PdX/AgOTf indicates that AgOTf facilitates some degree of X^-/OTf^- halide exchange.

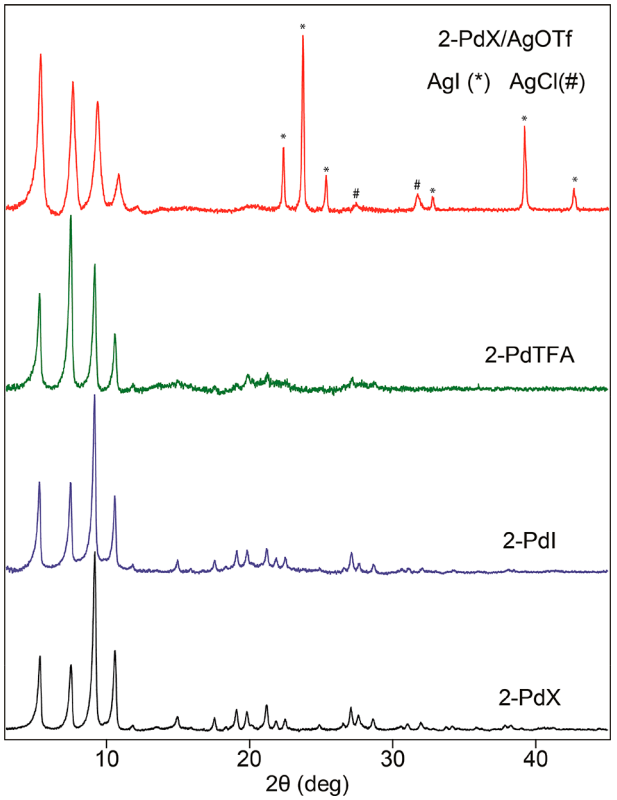

Figure 6. PXRD patterns of 2-PdX, 2-PdI, 2-PdTFA, and 2-PdX/AgOTf (Cu Kα, λ = 1.54 Å).

Catalytic Studies. Indoles are common motifs in natural products and pharmaceuticals.[49,50] They can be efficiently assembled using a variety of strategies, including Lewis acid-catalyzed intramolecular cyclization of *o*-alkynyl substituted anilines.[51] Moreover, Pd and Pt PNP pincer complexes have found success as Lewis acid catalysts for intramolecular hydrofunctionalization reactions.[52−59] In most cases, these catalysts are activated by exchanging halide ligands for more weakly coordinating anions. These considerations prompted us to compare the catalytic activity of the Pd P^NN^NP MOFs activated with $PhI(TFA)_2$ and AgOTf for intramolecular hydroamination reactions. 2-(Butyn-1-yl)aniline (**3**) was chosen as a benchmark substrate, and catalytic reactions were carried out in 1,4-dioxane at 95 °C with 5 mol % catalyst based on Pd (Table 1). Product yields were determined by integration of the ^1H NMR spectra.

Table 1. Hydroamination of *o*-Alkynyl Aniline 3[a,b]

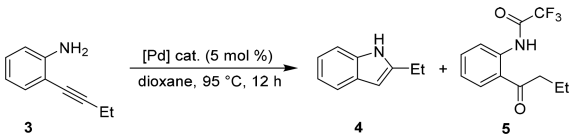

entry	catalyst	% yield 4	% yield 5	TON[c]
1	2-PdX	77		19
2	2-PdI	40		10
3	2-PdX/AgOTf	69		17
4	2-PdI/AgOTf	35		9
5	2-PdTFA	93	trace	23
6	2-PdTFA (run 2)	48		12
7	2-PdPMe_3	<5		<1
8	$^t\text{Bu}_4$L-PdOTf	94[d]		19
9	$^t\text{Bu}_4$L-PdTFA	52	5	10

[a]Reaction conditions: substrate (0.1 mmol), catalyst (0.005 mmol Pd), 1,4-dioxane, 95 °C, 12 h. [b]Yields were determined by ^1H NMR with respect to an internal standard (hexamethylbenzene). [c]Turnover numbers (TON) were calculated per Pd using the empirical formula for 2-PdX that accounts for missing linker defects. [d]Reaction time was 1 h.

Under the catalytic conditions, 2-PdX and 2-PdI afforded 2-ethylindole **4** in 77 and 40% yield, respectively (entries 1 and 2), after 12 h. 2-PdX exhibits remarkably good catalytic activity despite the presence of I^- and Cl^- ligands. The lower catalytic activity observed for 2-PdI is consistent with the presence of only the less labile I^- ligands. To our surprise, 2-PdX/AgOTf furnished **4** in slightly lower yield (69%) than 2-PdX. For comparison, a sample of 2-PdI/AgOTf was prepared by treating 2-PdI with AgOTf and found to deliver **4** in 35% yield under the same catalytic conditions. The similar catalytic activities of 2-PdX/AgOTf and 2-PdI/AgOTf to the parent MOFs 2-PdX and 2-PdI provide further support that AgOTf is not effective for X^-/OTf^- exchange at the Pd−X sites within these materials. Thus, formation of the AgX species observed by PXRD analysis should be the result of exchange of only the outer sphere halide counterions. Moreover, the slight decrease in catalytic activity of the AgOTf-treated MOFs compared to 2-PdX and 2-PdI may be attributed to pore occlusion by the insoluble AgX

DOI: 10.1021/acs.inorgchem.7b03063
Inorg. Chem. XXXX, XXX, XXX−XXX

species. 2-PdTFA proved to be the most active of the MOF catalysts, generating indole **4** in 93% yield (entry 5). The large difference in catalytic activity between 2-PdI/AgOTf and 2-PdTFA clearly illustrates the superiority of $PhITFA_2$ as an activating reagent. However, 2-PdTFA exhibits only modestly better activity than 2-PdX and significantly diminished activity upon attempted recycling (entry 6). Trace amounts of trifluoroacetamide **5** were also observed in the catalytic reactions employing 2-PdTFA. The consumption of TFA anions and a proton of unknown origin in this off-cycle reaction pathway may lead to catalyst deactivation and account for the modest activity and poor recyclability of 2-PdTFA. This notion is further supported by a marked difference in catalytic activity between the homogeneous complexes $^tBu_4$L-PdOTf and $^tBu_4$L-PdTFA (vide infra).

Given the evidence for a large number of defect sites in 2-PdX, we sought to confirm that the Pd pincer sites are responsible for the observed catalysis. We hypothesized that the strongly donating L-type ligand PMe_3 should selectively coordinate and block access to the Pd sites, shutting down the contribution of these sites to the observed catalysis. Consequently, 2-PdPMe_3 was synthesized by soaking 2-PdX in a MeCN solution of PMe_3. After washing, the $^{31}P\{^1H\}$ NMR spectrum of an acid-digested sample features a doublet and triplet resonance in a 2:1 ratio centered at 78.1 and δ −9.7 ppm ($^1J_{31P-P}$ = 25.7 Hz), respectively, that are assigned to H_4[L-Pd(PMe_3)]$^{2+}$ species (Figure S35). Signals attributed to H_4[L-PdI]$^+$ (74.0 ppm) and [$HPMe_3$]$^+$ (−2.90 ppm) also appear in a ∼1:1 ratio. The presence of the latter species indicates either incomplete conversion (∼75%) of the Pd−I sites to Pd−PMe_3 or PMe_3 ligand dissociation induced by the strongly acidic digestion procedure. Regardless, 2-PdPMe_3 delivered only trace amounts of **4** under the catalytic conditions (entry 7), substantiating that the Pd pincer sites are primarily responsible for catalysis. Similarly, catalytic reactions carried out in the presence of UiO−67 or absence of any catalyst showed no appreciable formation of the desired indole product.

The catalytic activities of the homogeneous complexes $^tBu_4$L-PdOTf and $^tBu_4$L-PdTFA were also investigated (Table 1, entries 8 and 9). $^tBu_4$L-PdOTf was markedly superior to 2-PdTFA, generating indole **4** in 94% yield after 1 h, while $^tBu_4$L-PdTFA furnished **4** in only 52% yield after 12 h. Similar to 2-PdTFA, a stoichiometric amount (∼5%) of trifluoroacetamide **5** was identified as a side product in the reaction employing $^tBu_4$L-PdTFA. Thus, we surmise that consumption of TFA^- via the formation of **5** leads to catalyst deactivation and is responsible for the poor activity of $^tBu_4$L-PdTFA and lack of recyclability of 2-PdTFA. Further studies are necessary to elucidate the mechanism of catalyst deactivation, but we hypothesize that the process stems from the greater basicity of TFA^- versus OTf^- and may involve deprotonation of the NH linker groups of the P^NN^NP ligand. This hypothesis would suggest that a more active and recyclable pincer MOF catalyst could be obtained by oxidative halide ligand exchange with a less basic anion such as OTf^-. However, attempts to carry out oxidative I^-/OTf^- exchange using in situ-generated $PhI(OTf)_2$ have been unsuccessful thus far, resulting in materials that suffer significant losses in crystallinity and exhibit poor catalytic activity. We believe this to be a limitation of the ill-defined nature of $PhI(OTf)_2$, which is usually generated in situ from $PhI(O_2CCH_3)_2$ and Me_3SiOTf.[60]

CONCLUSIONS

Carboxylate-functionalized Pd and Pt P^NN^NP pincer complexes were used for the assembly of porous Zr MOFs 2-PdX and 2-PtX. PXRD analysis shows that both MOFs adopt a cubic framework structure and are isostructural to the previously reported 1-PdX. This result is perhaps not surprising given the structural similarities between the P^NN^NP and P^OC^OP pincer ligand frameworks, but heralds the ability to synthesize isoreticular or multivariate MOFs using P^ZE^ZP pincer complexes. Despite similar solvothermal synthesis conditions, spectroscopic characterization and elemental analysis indicate that 2-PdX and 2-PtX contain a larger number of missing linker defects than 1-PdX and are best formulated as $\{Zr_6O_4(OH)_4(OAc)_{2.4}[PNNNP\text{-}MX]_{2.4}\}Y_{2.4}$ (X/Y = Cl, I).

Sequential treatment of 2-PdX with NaI and $PhI(TFA)_2$ generates 2-PdI and 2-PdTFA, respectively. The MOFs cleanly disassemble in trifluoroacetic acid, allowing for product characterization by solution state NMR and ESI-MS analysis. These analyses show complete Cl^-/I^- ligand exchange in 2-PdI and ∼50% conversion of the Pd−I sites to Pd−TFA in 2-PdTFA. The reaction of 2-PdX with AgOTf results in the formation of crystalline AgI and AgCl, but spectroscopic data suggest that X^-/OTf^- ligand exchange does not occur at the Pd−X sites. 2-PdTFA displays better catalytic activity than 2-PdI/AgOTf for the intramolecular hydroamination of 2-(butyn-1-yl)aniline, confirming that oxidative ligand exchange is a more effective means of activating the MOF-immobilized Pd species. 2-PdTFA also outperformed the homogeneous analogue $^tBu_4$L-PdTFA but is a less active catalyst than $^tBu_4$L-PdOTf. These results point to a detrimental effect of the trifluoroacetate ligands/anions on the Lewis acid catalytic activity of the Pd P^NN^NP complexes. Current studies are focused on developing new strategies to carry out halide ligand exchange with less basic and more weakly coordinating anions as well as expanding the scope of MOFs assembled from P^ZE^ZP pincer complexes.

EXPERIMENTAL SECTION

General Considerations. $ZrCl_4$ (Sigma-Aldrich), *N*,*N*-dimethylformamide (DMF, 99.9%, EMD), and glacial acetic acid (Macron) used for synthetic preparations were used as received unless otherwise noted. ClP(C_6H_5-COO^{t}Bu)$_2$,[22] $PdCl_2$(cod), $PtCl_2$(cod),[61] and butynyl aniline 3[62] were prepared as described in the literature. All other solvents and reagents were purchased from commercial suppliers and used as received. Routine powder X-ray diffraction patterns for phase identification were collected on a Rigaku Miniflex 600 diffractometer using Nickel-filtered Cu K_α radiation (λ = 1.5418 Å). High-resolution synchrotron PXRD data were collected at 295 K using beamline 11-BM at the Advanced Photon Source (APS, Argonne National Laboratory, Argonne, IL) using an average wavelength of 0.414536 Å. Nitrogen adsorption isotherms were measured at 77 K (liquid nitrogen bath) using a Micromeritics 3Flex Surface Characterization Analyzer. Prior to analysis, samples (100−200 mg) were heated under reduced pressure until the outgas rate was less than 2 mTorr/min. Inductively coupled plasma atomic emission spectroscopy (ICP-AES) measurements were performed by Robertson Microlit Laboratories (Ledgewood, NJ). Elemental microanalyses were performed by Atlantic Microlab (Norcross, GA) or Robertson Microlit Laboratories (Ledgewood, NJ). ESI-MS experiments were performed using a Micromass ZQ4000 single quadrupole mass detector.

Solution-state NMR spectra were measured using either a Varian Inova or MR 400 MHz spectrometer (101 MHz operating frequency for ^{13}C, 162 MHz operating frequency for ^{31}P, and 376 MHz operating frequency for ^{19}F). For ^1H and $^{13}C\{^1H\}$ NMR spectra, the solvent resonance was referenced as an internal standard. For $^{31}P\{^1H\}$ NMR spectra, 85% H_3PO_4 was used as an external standard (0 ppm). For ^{19}F

DOI: 10.1021/acs.inorgchem.7b03063
Inorg. Chem. XXXX, XXX, XXX−XXX

NMR spectra, 1% CF_3COOH was used as an external standard (−76.55 ppm). Solvent-suppressed ^1H NMR spectra were collected using the WET1D sequence with default parameters.[63] Solid-state NMR experiments were performed on a Bruker (Billerica, MA) DSX-400 spectrometer at a resonance frequency of 400 MHz for ^1H and 162 MHz for ^{31}P and 100 MHz for ^{13}C using a MAS probe in double-resonance mode. See Supporting Information for additional details.

Synthesis of ^{t}Bu$_4$L. Under an inert atmosphere, a 100 mL Schlenk flask was charged with 2,6-diaminopyridine (0.156 g, 1.43 mmol), triethylamine (0.360 g, 3.56 mmol), and toluene (25 mL). The reaction mixture was cooled to 0 °C, and a solution of ClP-$(C_6H_4COO^{tBu})_2$ (1.344 g, 3.19 mmol) in toluene (20 mL) was added dropwise. The flask was then sealed and heated at 80 °C for 16 h. After cooling, the pale yellow solution was filtered, and the solvent was removed under reduced pressure. The resulting sticky yellow powder was recrystallized with toluene:pentane (1:4) to give the desired product as a white microcrystalline powder (1.04 g, 1.18 mmol, 83%). $^{31}P\{^1H\}$ NMR (162.0 MHz, $CDCl_3$): δ 25.4 (s). ^1H NMR (400 MHz, $CDCl_3$): δ 7.95 (d, J = 7.7 Hz, 8H), 7.46 (t, J = 7.6 Hz, 8H), 7.34 (t, J = 8.0 Hz, 1H), 6.44 (d, J = 7.8 Hz, 2H), 4.99 (d, J = 7.6 Hz, 2H), 1.58 (s, 36H). $^{13}C\{^1H\}$ NMR (101 MHz, $CDCl_3$): δ 165.4 (s, 4C, CO_2), 157.2 (d, J = 20.5 Hz, 2C, $Py^{2,6}$), 144.4 (d, J = 14.4 Hz, 4C, Ph), 140.0 (s, C, Py^4), 133.0 (s, 4C, Ph^4), 131.1 (d, 8C, J = 21.0 Hz, $Ph^{2,6}$), 129.5 (d, 8C, J = 6.6 Hz, $Ph^{3,5}$), 99.9 (d, 2C, J = 14.4 Hz, 2C, $Py^{3,5}$), 81.4 (s, 4C, $C(CH_3)_3$), 28.3 (s, 12C, $C(CH_3)_3$). $^{31}P\{^1H\}$ NMR (162.0 MHz, $CDCl_3$): δ 25.4 (s). Anal. Calcd for $C_{49}H_{57}N_3O_8P_2$: C, 67.04; H, 6.54; N, 4.79; Found: C, 67.30; H, 6.55; N, 4.83.

Synthesis of ^{t}Bu$_4$L-PdCl. A solution of $PdCl_2$(cod) (0.164 g, 0.575 mmol) in CH_2Cl_2 (3 mL) was added to a stirring solution of ^{t}Bu$_4$L (0.505 g, 0.575 mmol) in CH_2Cl_2 (8 mL). The reaction was stirred at room temperature for 4 h under an inert atmosphere before the volatiles were removed under reduced pressure. The resulting orange residue was triturated with a small amount of pentane (3 mL), resulting in formation of a bright yellow solid. The solid was collected by filtration, washed with pentane (3 × 3 mL), and dried under reduced pressure to yield ^{t}Bu$_4$L-PdCl (0.574 g, 95% yield). ^1H NMR (400 MHz, $CDCl_3$): δ 11.17 (s, 2H, N*H*), δ 8.10 (dd, $^3J_{H-P}$ = 14.2 Hz, $^3J_{H-H}$ = 6.4 Hz, 8H, benzoate Ar−H), 7.92 (d, $^3J_{H-H}$ = 8.1 Hz, 8H, benzoate Ar−H), 7.18 (t, $^3J_{H-H}$ = 6.4 Hz, 1H, pyridine Ar−H), 7.11 (d, $^3J_{H-H}$ = 7.8 Hz, 2H, pyridine Ar−H), 1.50 (s, 36H, ^{t}Bu). $^{13}C\{^1H\}$ NMR (101 MHz, $CDCl_3$): δ 164.3 (s, 4C, CO_2), 160.9 (t, J_{C-P} = 7.7 Hz, 2C, Ar), 142.6 (s, C, Ar), 135.5 (s, 4C, Ar), 134.0 (t, J_{C-P} = 28.6 Hz, 4C, Ar), 132.2 (t, J_{C-P} = 8.1 Hz, 8C, Ar), 130.0 (t, J_{C-P} = 6.1 Hz, 8C, Ar), 102.2 (br, 2C, Ar), 81.9 (s, 4C, $C(CH_3)_3$), 28.2 (s, 12C, $C(CH_3)_3$). $^{31}P\{^1H\}$ NMR (162.0 MHz, $CDCl_3$): δ 67.8 (s). Anal. Calcd for $C_{49}H_{57}Cl_2N_3O_8P_2Pd$: C, 55.77; H, 5.44; N, 3.98; Found: C, 55.96; H, 5.61; N, 3.79.

Synthesis of ^{t}Bu$_4$L-PtCl. The compound was prepared from $PtCl_2$(cod) (0.277 g, 0.740 mmol) and ^{t}Bu$_4$L (0.656 g, 0.747 mmol) following the same procedure used for ^{t}Bu$_4$L-PdCl. The reaction yielded 0.806 g (0.705 mmol, 95%) of ^{t}Bu$_4$L-PtCl as a bright yellow solid. ^1H NMR (400 MHz, $CDCl_3$): δ 11.57 (s, 2H, N*H*), 8.10 (dd, $^3J_{H-P}$ = 13.8 Hz, $^3J_{H-H}$ = 6.8 Hz, 8H, benzoate Ar−H), 7.95 (d, $^3J_{H-H}$ = 7.9 Hz, 8H, benzoate Ar−H), 7.08 (m, br, 3H, pyridine Ar−H), 1.51 (s, 36H, ^{t}Bu). $^{13}C\{^1H\}$ NMR (101 MHz, $CDCl_3$): δ 164.4 (s, 4C, CO_2), 160.7 (t, J_{C-P} = 6.9 Hz, 2C, Ar), 141.5 (s, C, Ar), 135.6 (s, 4C, Ar), 134.2 (t, J_{C-P} = 33.1 Hz, 4C, Ar), 132.4 (t, J_{C-P} = 8.0 Hz, 8C, Ar), 130.0 (t, J_{C-P} = 6.3 Hz, 8C, Ar), 101.6 (br, 2C, Ar), 82.0 (s, 4C, $C(CH_3)_3$), 28.2 (s, 12C, $C(CH_3)_3$). $^{31}P\{^1H\}$ NMR (162.0 MHz, $CDCl_3$): δ 61.9 (d, $^1J_{Pt-P}$ = 2770 Hz). Anal. Calcd for $C_{49}H_{57}Cl_2N_3O_8P_2Pt$: C, 51.45; H, 5.02; N, 3.67; Found: C, 51.39; H, 5.06; N, 3.54.

Synthesis of ^{t}Bu$_4$L-PdI. A solution of ^{t}Bu$_4$L-PdCl (1.105 g, 1.05 mmol) in acetone (8 mL) was treated with a solution of NaI (0.317 g, 2.12 mmol) in acetone (1 mL). Immediate formation of NaCl was observed, and the reaction was allowed to stir at room temperature for 1 h. The solvent was removed under reduced pressure, and the dark red residue was extracted with CH_2Cl_2 (5 mL) and filtered through a 0.45 μm PTFE syringe filter. The filtrate was concentrated in vacuo to afford the desired product as an orange solid (1.248 g, 96%). ^1H NMR (400 MHz, $CDCl_3$): δ 9.60 (s, 2H, N*H*), 8.09−7.99 (m, 16H, benzoate Ar−H), 7.40 (t, $^3J_{H-H}$ = 7.5 Hz, 1H, pyridine Ar−H), 7.30 (d, $^3J_{H-H}$ = 8.2 Hz, 2H, pyridine Ar−H), 1.53 (s, 36H, ^{t}Bu). $^{13}C\{^1H\}$ NMR (101 MHz, $CDCl_3$): δ 164.4 (s, 4C, CO_2), 159.7 (t, J_{C-P} = 7.2 Hz, 2C, Ar), 142.6 (s, C, Ar), 136.0 (s, 4C, Ar), 133.44 (t, J_{C-P} = 8.0 Hz, 8C, Ar), 133.40 (t, J_{C-P} = 29.4 Hz, 4C, Ar), 130.0 (t, J_{C-P} = 6.1 Hz, 8C, Ar), 102.3 (br, 2C, Ar), 82.1 (s, 4C, $C(CH_3)_3$), 28.2 (s,12C, $C(CH_3)_3$). $^{31}P\{^1H\}$ NMR (162.0 MHz, $CDCl_3$): δ 75.6 (s). Anal. Calcd for $C_{49}H_{57}I_2N_3O_8P_2Pd$: C, 47.53; H, 4.64; N, 3.39; Found: C, 47.57; H, 4.79; N, 3.45;

Synthesis of ^{t}Bu$_4$L-PtI. The compound was prepared from ^{t}Bu$_4$L-PtCl (0.863 g, 0.754 mmol) following the same procedure used for ^{t}Bu$_4$L-PdI. The reaction yielded 0.951 g (95%) of ^{t}Bu$_4$L-PtI as a reddish-orange solid. ^1H NMR (400 MHz, $CDCl_3$): δ 10.09 (s, 2H), 8.09−7.99 (m, 16H, benzoate Ar−H), 7.42 (t, $^3J_{H-H}$ = 7.7 Hz, 1H, pyridine Ar−H), 7.31 (d, $^3J_{H-H}$ = 8.0 Hz, 2H, pyridine Ar−H), 1.53 (s, 36H, ^{t}Bu). $^{13}C\{^1H\}$ NMR (101 MHz, $CDCl_3$): δ 164.4 (s, 4C, CO_2), 159.6 (t, J_{C-P} = 6.6 Hz, 2C, Ar), 141.7 (s, C, Ar), 136.0 (s, 4C, Ar), 133.6 (t, J_{C-P} = 7.8 Hz, 8C, Ar), 133.1 (t, J_{C-P} = 33.9 Hz, 4C, Ar), 129.9 (t, J_{C-P} = 6.3 Hz, 8C, Ar), 101.8 (br, 2C, Ar), 82.1 (s, 4C, $C(CH_3)_3$), 28.2 (s, 12C, $C(CH_3)_3$). $^{31}P\{^1H\}$ NMR (162.0 MHz, $CDCl_3$): δ 68.1 (d, $^1J_{Pt-P}$ = 2682.8 Hz). Anal. Calcd for $C_{49}H_{57}I_2N_3O_8P_2Pt$: C, 44.36; H, 4.33; N, 3.17; Found: C, 44.31; H, 4.52; N, 3.14.

Synthesis of H$_3$L-PdI. Trifluoroacetic acid (1 mL) was added to a solution of ^{t}Bu$_4$L-PdI (0.542 g, 0.438 mmol) in CH_2Cl_2 (5 mL), resulting in a color change of the solution from ruby to dark purple. The solution was stirred for 16 h at room temperature before removing the solvent using a rotary evaporator. Deionized water (12 mL) was added, resulting in precipitation of a bright orange solid. The solid was collected by vacuum filtration and washed with deionized water (3 × 5 mL) and $CHCl_3$ (~20 mL). The solid was dried under reduced pressure to afford 0.393 g of the crude product (H_4[L-PdI]I). The solid was suspended in acetone (5 mL), and a solution of pyridine (0.032 g, 0.405 mmol) in acetone (2 mL) was added, resulting in a color change of the supernatant from ruby to bright orange. The solution was stirred for 30 min at room temperature. The mixture was centrifuged, and the supernatant was decanted. The solid was washed successively with acetone (3 × 5 mL) and then water (~20 mL) until no color persisted in the filtrate. The resulting bright orange solid was dried under vacuum to afford H_3[L-PdI] (0.284 g, 0.321 mmol, 86% yield). ^1H NMR (400 MHz, DMSO): δ 12.71 (br, 2H, N*H*), 8.07 (d, $^3J_{H-H}$ = 7.8 Hz, 8H, benzoate Ar−H), δ 7.94 (dd, $^3J_{H-P}$ = 12.9 Hz, $^3J_{H-H}$ = 6.1 Hz, 8H, benzoate Ar−H), 7.41 (t, $^3J_{H-H}$ = 7.7 Hz, 1H, pyridine Ar−H), 6.28 (d, $^3J_{H-H}$ = 7.2 Hz, 2H, pyridine Ar−H). $^{13}C\{^1H\}$ NMR (101 MHz, DMSO): δ 166.7 (s, 4C, CO_2), 162.9 (br, 2C, Ar), 141.8 (br, C, Ar), 136.4 (br, 4C, Ar), 134.3 (br, 8C, Ar), 132.5 (dd, J_{C-P} = 13.0 Hz, J_{C-P} = 6.4 Hz, 4C, Ar), 129.5 (t, J_{C-P} = 5.4 Hz, 8C, Ar), 98.8 (br, 2C, Ar). $^{31}P\{^1H\}$ NMR (162.0 MHz, DMSO): δ 69.9 (s). Anal. Calcd for H_3L-PdI·(H_2O); $C_{33}H_{26}IN_3O_9P_2Pd$: C, 43.85; H, 2.90; N, 4.65; Found: C, 44.18; H, 3.07; N, 4.55.

Synthesis of H$_3$L-PtI. The compound was prepared from ^{t}Bu$_4$L-PtI (0.748 g) following the same procedure used for H_3L-PdI. The reaction yielded 0.454 g (90%) of H_3L-PtI as an orange solid. ^1H NMR (400 MHz, DMSO): δ 12.23 (br, 2H, N*H*), δ 8.09 (d, $^3J_{H-H}$ = 7.8 Hz, 8H, benzoate Ar−H), 7.93 (dd, $^3J_{H-P}$ = 13.4, $^3J_{H-H}$ = 6.1 Hz, 8H, benzoate Ar−H), 7.47 (t, $^3J_{H-H}$ = 7.8 Hz, 1H, pyridine Ar−H), 6.34 (d, $^3J_{H-H}$ = 7.5 Hz, 2H, pyridine Ar−H). $^{13}C\{^1H\}$ NMR (101 MHz, DMSO): δ 166.6 (s, 4C, CO_2), 140.8 (s, C, Ar), 134.2 (s, 4C, Ar), 137.0 (t, J_{C-P} = 36.8 Hz, 4C, Ar), 132.5 (t, $^3J_{C-P}$ = 7.1 Hz, 8C, Ar), 129.5 (t, J_{C-P} = 5.7 Hz, 8C, Ar), 97.9 (s, 2C, Ar). $^{31}P\{^1H\}$ NMR (162.0 MHz, DMSO): δ 63.2 (d, $^1J_{Pt-P}$ = 2561.4 Hz). Anal. Calcd for H_3(PNNNP)PtI; $C_{33}H_{24}IN_3O_8P_2Pt$: C, 40.67; H, 2.48; N, 4.31; Found: C, 40.57; H, 2.67; N, 4.26.

Synthesis of 2-PdX and 2-PtX. Anhydrous $ZrCl_4$ (0.030 g, 0.129 mmol) was suspended in acetic acid (1.6 mL) and DMF (4.4 mL) in a 20 mL screw-top scintillation vial. A solution of H_3L-PdI or H_3L-PtI (0.043 mmol) in DMF (2 mL) was added, and the vial was sealed with

DOI: 10.1021/acs.inorgchem.7b03063
Inorg. Chem. XXXX, XXX, XXX−XXX

Teflon-lined screw-top cap (Qorpak CAP-00554). The reaction mixture was sonicated for 5 min to ensure complete dissolution of the solids. The vial was then placed in a programmable oven at room temperature and heated to 120 °C for 16 h. After reaching room temperature, the solvent was decanted from the precipitated solid. The solid was washed with DMF (3 × 15 mL) and acetone (3 × 10 mL) and dried in vacuo (0.01 Torr) at room temperature for 2 h to afford 0.035 g of product. 2-PdX: $^{31}P\{^{1}H\}$ NMR (162.0 MHz, 3/1 v/v CF_3COOH/C_6D_6): δ 74.0 (s); 69.9 (s). Anal. Calcd for $\{Zr_6O_4(OH)_4[PdClC_{33}H_{21}N_3O_8P_2]_{2.4}(CH_3COO)_{2.4}\}I_{2.4}$; C, 34.68; H, 2.16; N, 3.37; I, 10.18; Cl, 2.84, Zr, 17.68; Pd, 8.54; Found: C, 32.70; H, 2.47; N, 3.11; I, 6.54; Cl, 1.95; Zr, 16.60; Pd, 6.68. 2-PtX: $^{31}P\{^{1}H\}$ NMR (162.0 MHz, 3/1 v/v CF_3COOH/C_6D_6): δ 67.7 ($^{1}J_{Pt-P}$ = 2719 Hz,); 64.0 ($^{1}J_{Pt-P}$ = 2790 Hz,). Anal. Calcd for $Zr_6O_4(OH)_4[PtClC_{33}H_{21}N_3O_8P_2]_{2.4}(CH_3COO)_{2.4}\}I_{2.4}$; C, 32.14; H, 2.00; N, 3.12; I, 9.43; Cl, 2.64; Zr, 16.95; Pt, 14.50; Found: C, 32.05; H, 2.27; N, 3.49; I, 5.19; Cl, 1.62; Zr, 15.32; Pt, 12.11.

Synthesis of 2-PdI. A solution of NaI (0.098 g, 0.655 mmol) in deionized water (5 mL) was added to a suspension of 2-PdX (0.160 g) in deionized water (5 mL) in a 20 mL scintillation vial. The vial was sealed and placed in an oven at 60 °C for 2 h. After cooling, the mixture was centrifuged, and the supernatant was decanted. A fresh solution of NaI (0.098 g, 0.655 mmol) in deionized water (5 mL) was added, and the reaction was again heated at 60 °C for 2 h. The solid was collected by centrifugation and washed successively with water (3 × 10 mL) and acetone (3 × 10 mL) and dried briefly in vacuo to afford 2-PdI as a yellow microcrystalline powder (0.150 g). $^{31}P\{^{1}H\}$ NMR (162.0 MHz, 3/1 v/v CF_3COOH/C_6D_6): δ 74.0 (s).

Synthesis of 2-PdTFA. In a N_2-filled glovebox, solution of $PhITFA_2$ (0.026 g, 0.06 mmol) in CH_2Cl_2 (1 mL) was added to a suspension of 2-PdI (0.050 g) in CH_2Cl_2 (5 mL) in a 20 mL scintillation vial. The vial was sealed and left gently stirring at room temperature. After 12 h, the reaction mixture was centrifuged, and the pink purple supernatant was decanted. The solid was washed with CH_2Cl_2 (3 × 5 mL) and dried briefly in vacuo. 2-PdTFA was isolated as a pale yellow, microcrystalline powder (0.050 mg). $^{31}P\{^{1}H\}$ NMR (162.0 MHz, 3/1 v/v CF_3COOH/C_6D_6): δ 74.0 (s); 71.1 (s).

Reaction of 2-PdX and 2-PdI with AgOTf. In a N_2-filled glovebox, a solution of AgOTf (0.023 g, 0.090 mmol) in MeCN (1 mL) was added to a suspension of 2-PdX or 2-PdI (0.050 g) in MeCN (5 mL) in a 20 mL scintillation vial. The vial was sealed and left gently stirring at 60 °C. After 12 h, the reaction mixture was centrifuged, and the supernatant was decanted. The solid was washed with MeCN (3 × 5 mL) and dried briefly in vacuo. 2-PdX/AgOTf and 2-PdI/AgOTf were isolated as yellow microcrystalline powders (0.050 g).

Synthesis of 2-Pd(PMe_3). In a N_2-filled glovebox, a solution of PMe_3 (0.097 g, 1.27 mmol) in MeCN (1 mL) was added to a suspension of 2-PdX (0.020 g) in MeCN (2 mL) in a 20 mL scintillation vial. The vial was sealed and left gently stirring at room temperature. After 12 h, the reaction mixture was centrifuged, and the supernatant was decanted. The solid was washed with MeCN (3 × 5 mL) and dried briefly in vacuo. 2-Pd(PMe_3) was isolated as a yellow microcrystalline powder (0.020 mg). $^{31}P\{^{1}H\}$ NMR (162.0 MHz, 3/1 v/v CF_3COOH/C_6D_6): δ 78.1 (d, $^{1}J_{P-P}$ = 25.7 Hz, $H_4[L\text{-}Pd(PMe_3)]^{2+}$) 74.0 (s, $H_4[L\text{-}PdI]^{+}$); 2.9 (s, $HPMe_3^{+}$); −9.7 (t, $^{1}J_{P-P}$ = 25.7 Hz, $H_4[L\text{-}Pd(PMe_3)]^{2+}$).

General Procedure for Intramolecular Hydroamination Reactions. In a N_2-filled glovebox, a vial was charged with **3** (0.1 mmol), 5 mol % catalyst, 1,4-dioxane (0.4 mL), C_6D_6 (0.1 mL), and a known amount of hexamethylbenzene (0.02−0.04 mmol) as an internal standard. The reaction mixture was transferred to an NMR tube and heated at 95 °C for 12 h. The product yields were determined by ^{1}H NMR spectroscopy.

■ ASSOCIATED CONTENT

Supporting Information

The Supporting Information is available free of charge on the ACS Publications website at DOI: 10.1021/acs.inorgchem.7b03063.

Spectroscopic (NMR, IR) and ESI-MS data and crystallographic data collection and refinement details for H_3L-PdI (PDF)

Accession Codes

CCDC 1587001 contains the supplementary crystallographic data for this paper. These data can be obtained free of charge via www.ccdc.cam.ac.uk/data_request/cif, by emailing data_request@ccdc.cam.ac.uk, or by contacting The Cambridge Crystallographic Data Centre, 12 Union Road, Cambridge CB2 1EZ, UK; fax: +44 1223 336033.

■ AUTHOR INFORMATION

Corresponding Author

*E-mail: wade.521@osu.edu.

ORCID

Klaus Schmidt-Rohr: 0000-0002-3188-4828

Bruce M. Foxman: 0000-0001-5707-8341

Casey R. Wade: 0000-0002-7044-9749

Present Address

‡C.R.W.: Department of Chemistry and Biochemistry, The Ohio State University, Columbus, Ohio 43210, United States.

Notes

The authors declare no competing financial interest.

■ ACKNOWLEDGMENTS

Acknowledgment is made to the Donors of the American Chemical Society Petroleum Research Fund (Grant 55281-DNI-3) for support of this research. Use of the Advanced Photon Source at Argonne National Laboratory was supported by the U.S. Department of Energy (DOE) Office of Science under Contract DE-AC02-06CH11357.

■ REFERENCES

(1) Benito-Garagorri, D.; Kirchner, K. Modularly designed transition metal PNP and PCP pincer complexes based on aminophosphines: synthesis and catalytic applications. *Acc. Chem. Res.* **2008**, *41*, 201−213.

(2) Selander, N.; Szabó, K. J. Catalysis by Palladium Pincer Complexes. *Chem. Rev.* **2011**, *111*, 2048−2076.

(3) Zhang, H.; Lei, A. Palladium(IV) chemistry supported by pincer type ligands. *Dalton Trans.* **2011**, *40*, 8745−8745.

(4) Gunanathan, C.; Milstein, D. Bond activation and catalysis by ruthenium pincer complexes. *Chem. Rev.* **2014**, *114*, 12024−12087.

(5) Younus, H. A.; Ahmad, N.; Su, W.; Verpoort, F. Ruthenium pincer complexes: Ligand design and complex synthesis. *Coord. Chem. Rev.* **2014**, *276*, 112−152.

(6) Zell, T.; Milstein, D. Hydrogenation and dehydrogenation iron pincer catalysts capable of metal-ligand cooperation by aromatization/dearomatization. *Acc. Chem. Res.* **2015**, *48*, 1979−1994.

(7) Younus, H. A.; Su, W.; Ahmad, N.; Chen, S.; Verpoort, F. Ruthenium Pincer Complexes: Synthesis and Catalytic Applications. *Adv. Synth. Catal.* **2015**, *357*, 283−330.

(8) Bauer, G.; Hu, X. Recent developments of iron pincer complexes for catalytic applications. *Inorg. Chem. Front.* **2016**, *3*, 741−765.

(9) Kumar, A.; Bhatti, T. M.; Goldman, A. S. Dehydrogenation of Alkanes and Aliphatic Groups by Pincer-Ligated Metal Complexes. *Chem. Rev.* **2017**, *117*, 12357−12384.

(10) Garbe, M.; Junge, K.; Beller, M. Homogeneous Catalysis by Manganese-Based Pincer Complexes. *Eur. J. Org. Chem.* **2017**, *2017*, 4344−4362.

(11) Tanaka, R.; Yamashita, M.; Nozaki, K. Catalytic Hydrogenation of Carbon Dioxide Using Ir(III)-Pincer Complexes. *J. Am. Chem. Soc.* **2009**, *131*, 14168−14169.

DOI: 10.1021/acs.inorgchem.7b03063
Inorg. Chem. XXXX, XXX, XXX−XXX

(12) Arashiba, K.; Miyake, Y.; Nishibayashi, Y. A molybdenum complex bearing PNP-type pincer ligands leads to the catalytic reduction of dinitrogen into ammonia. *Nat. Chem.* **2011**, *3*, 120−125.
(13) Kang, P.; Meyer, T. J.; Brookhart, M. Selective electrocatalytic reduction of carbon dioxide to formate by a water-soluble iridium pincer catalyst. *Chem. Sci.* **2013**, *4*, 3497−3502.
(14) Filonenko, G. A.; van Putten, R.; Schulpen, E. N.; Hensen, E. J. M.; Pidko, E. A. Highly Efficient Reversible Hydrogenation of Carbon Dioxide to Formates Using a Ruthenium PNP-Pincer Catalyst. *ChemCatChem* **2014**, *6*, 1526−1530.
(15) Scheuermann, M. L.; Semproni, S. P.; Pappas, I.; Chirik, P. J. Carbon dioxide hydrosilylation promoted by cobalt pincer complexes. *Inorg. Chem.* **2014**, *53*, 9463−9465.
(16) Rosler, S.; Obenauf, J.; Kempe, R. A Highly Active and Easily Accessible Cobalt Catalyst for Selective Hydrogenation of C-O Bonds. *J. Am. Chem. Soc.* **2015**, *137*, 7998−8001.
(17) Mastalir, M.; Glatz, M.; Pittenauer, E.; Allmaier, G.; Kirchner, K. Sustainable Synthesis of Quinolines and Pyrimidines Catalyzed by Manganese PNP Pincer Complexes. *J. Am. Chem. Soc.* **2016**, *138*, 15543−15546.
(18) Ma, Q. Q.; Liu, T.; Li, S.; Zhang, J.; Chen, X.; Guan, H. Highly efficient reduction of carbon dioxide with a borane catalyzed by bis(phosphinite) pincer ligated palladium thiolate complexes. *Chem. Commun.* **2016**, *52*, 14262−14265.
(19) Anaby, A.; Feller, M.; Ben-David, Y.; Leitus, G.; Diskin-Posner, Y.; Shimon, L. J.; Milstein, D. Bottom-Up Construction of a CO2-Based Cycle for the Photocarbonylation of Benzene, Promoted by a Rhodium(I) Pincer Complex. *J. Am. Chem. Soc.* **2016**, *138*, 9941−9950.
(20) Bertini, F.; Glatz, M.; Gorgas, N.; Stoger, B.; Peruzzini, M.; Veiros, L. F.; Kirchner, K.; Gonsalvi, L. Carbon dioxide hydrogenation catalysed by well-defined Mn(I) PNP pincer hydride complexes. *Chem. Sci.* **2017**, *8*, 5024−5029.
(21) Adams, G. M.; Weller, A. S. POP-type ligands: Variable coordination and hemilabile behaviour. *Coord. Chem. Rev.* **2018**, *355*, 150−172.
(22) Burgess, S. A.; Kassie, A.; Baranowski, S. A.; Fritzsching, K. J.; Schmidt-Rohr, K.; Brown, C. M.; Wade, C. R. Improved Catalytic Activity and Stability of a Palladium Pincer Complex by Incorporation into a Metal-Organic Framework. *J. Am. Chem. Soc.* **2016**, *138*, 1780−1783.
(23) He, J.; Waggoner, N. W.; Dunning, S. G.; Steiner, A.; Lynch, V. M.; Humphrey, S. M. A PCP Pincer Ligand for Coordination Polymers with Versatile Chemical Reactivity: Selective Activation of CO2 Gas over CO Gas in the Solid State. *Angew. Chem., Int. Ed.* **2016**, *55*, 12351−12355.
(24) Rimoldi, M.; Nakamura, A.; Vermeulen, N. A.; Henkelis, J. J.; Blackburn, A. K.; Hupp, J. T.; Stoddart, J. F.; Farha, O. K. A metal−organic framework immobilised iridium pincer complex. *Chem. Sci.* **2016**, *7*, 4980−4984.
(25) He, J.; Bohnsack, A. M.; Waggoner, N. W.; Dunning, S. G.; Lynch, V. M.; Kaska, W. C.; Humphrey, S. M. 1-D and 2-D phosphine coordination materials based on a palladium(II) PCP pincer metalloligand. *Polyhedron* **2017**, 1.
(26) Lee, J.; Farha, O. K.; Roberts, J.; Scheidt, K. A.; Nguyen, S. T.; Hupp, J. T. Metal-organic framework materials as catalysts. *Chem. Soc. Rev.* **2009**, *38*, 1450−1459.
(27) Wang, C.; Liu, D.; Lin, W. Metal-organic frameworks as a tunable platform for designing functional molecular materials. *J. Am. Chem. Soc.* **2013**, *135*, 13222−13234.
(28) Chughtai, A. H.; Ahmad, N.; Younus, H. A.; Laypkov, A.; Verpoort, F. Metal-organic frameworks: versatile heterogeneous catalysts for efficient catalytic organic transformations. *Chem. Soc. Rev.* **2015**, *44*, 6804−6849.
(29) Cohen, S. M.; Zhang, Z.; Boissonnault, J. A. Toward "metalloMOFzymes": Metal-Organic Frameworks with Single-Site Metal Catalysts for Small-Molecule Transformations. *Inorg. Chem.* **2016**, *55*, 7281−7290.
(30) Rogge, S. M. J.; Bavykina, A.; Hajek, J.; Garcia, H.; Olivos-Suarez, A. I.; Sepulveda-Escribano, A.; Vimont, A.; Clet, G.; Bazin, P.; Kapteijn, F.; Daturi, M.; Ramos-Fernandez, E. V.; Llabres i Xamena, F. X.; Van Speybroeck, V.; Gascon, J. Metal-organic and covalent organic frameworks as single-site catalysts. *Chem. Soc. Rev.* **2017**, *46*, 3134−3184.
(31) Gui, B.; Meng, X.; Chen, Y.; Tian, J.; Liu, G.; Shen, C.; Zeller, M.; Yuan, D.; Wang, C. Reversible Tuning Hydroquinone/Quinone Reaction in Metal−Organic Framework: Immobilized Molecular Switches in Solid State. *Chem. Mater.* **2015**, *27*, 6426−6431.
(32) Meng, X.; Gui, B.; Yuan, D.; Zeller, M.; Wang, C. Mechanized azobenzene-functionalized zirconium metal-organic framework for on-command cargo release. *Sci. Adv.* **2016**, *2*, e1600480.
(33) Choi, J.; MacArthur, A. H. R.; Brookhart, M.; Goldman, A. S. Dehydrogenation and Related Reactions Catalyzed by Iridium Pincer Complexes. *Chem. Rev.* **2011**, *111*, 1761−1779.
(34) Nawara-Hultzsch, A. J.; Hackenberg, J. D.; Punji, B.; Supplee, C.; Emge, T. J.; Bailey, B. C.; Schrock, R. R.; Brookhart, M.; Goldman, A. S. Rational design of highly active "hybrid" phosphine−phosphinite pincer iridium catalysts for alkane metathesis. *ACS Catal.* **2013**, *3*, 2505−2514.
(35) Shaffer, D. W.; Johnson, S. I.; Rheingold, A. L.; Ziller, J. W.; Goddard, W. A.; Nielsen, R. J.; Yang, J. Y. Reactivity of a series of isostructural cobalt pincer complexes with CO2, CO, and H(+). *Inorg. Chem.* **2014**, *53*, 13031−13041.
(36) Benito-Garagorri, D.; Becker, E.; Wiedermann, J.; Lackner, W.; Pollak, M.; Mereiter, K.; Kisala, J.; Kirchner, K. Achiral and Chiral Transition Metal Complexes with Modularly Designed Tridentate PNP Pincer-Type Ligands Based on N-Heterocyclic Diamines. *Organometallics* **2006**, *25*, 1900−1913.
(37) Cattalini, L.; Cusumano, M.; Ricevuto, V.; Trozzi, M. Fast reactions at planar four-co-ordinate complexes. Part II. The leaving-group effect in palladium(II) complexes of 3-azapentane-1,5-diamine. *J. Chem. Soc., Dalton Trans.* **1975**, 771−774.
(38) Katz, M. J.; Brown, Z. J.; Colón, Y. J.; Siu, P. W.; Scheidt, K. A.; Snurr, R. Q.; Hupp, J. T.; Farha, O. K. A facile synthesis of UiO-66, UiO-67 and their derivatives. *Chem. Commun.* **2013**, *49*, 9449−9449.
(39) Oien, S.; Wragg, D.; Reinsch, H.; Svelle, S.; Bordiga, S.; Lamberti, C.; Lillerud, K. P. Detailed Structure Analysis of Atomic Positions and Defects in Zirconium Metal-Organic Frameworks. *Cryst. Growth Des.* **2014**, *14*, 5370−5372.
(40) Shearer, G. C.; Chavan, S.; Ethiraj, J.; Vitillo, J. G.; Svelle, S.; Olsbye, U.; Lamberti, C.; Bordiga, S.; Lillerud, K. P. Tuned to Perfection: Ironing Out the Defects in Metal−Organic Framework UiO-66. *Chem. Mater.* **2014**, *26*, 4068−4071.
(41) Trickett, C. A.; Gagnon, K. J.; Lee, S.; Gándara, F.; Bürgi, H. B.; Yaghi, O. M. Definitive Molecular Level Characterization of Defects in UiO-66 Crystals. *Angew. Chem., Int. Ed.* **2015**, *54*, 11162−11167.
(42) Wu, H.; Chua, Y. S.; Krungleviciute, V.; Tyagi, M.; Chen, P.; Yildirim, T.; Zhou, W. Unusual and Highly Tunable Missing-Linker Defects in Zirconium Metal−Organic Framework UiO-66 and Their Important Effects on Gas Adsorption. *J. Am. Chem. Soc.* **2013**, *135*, 10525−10532.
(43) Atzori, C.; Shearer, G. C.; Maschio, L.; Civalleri, B.; Bonino, F.; Lamberti, C.; Svelle, S.; Lillerud, K. P.; Bordiga, S. Effect of Benzoic Acid as a Modulator in the Structure of UiO-66: An Experimental and Computational Study. *J. Phys. Chem. C* **2017**, *121*, 9312−9324.
(44) Shearer, G. C.; Chavan, S.; Bordiga, S.; Svelle, S.; Olsbye, U.; Lillerud, K. P. Defect Engineering: Tuning the Porosity and Composition of the Metal−Organic Framework UiO-66 via Modulated Synthesis. *Chem. Mater.* **2016**, *28*, 3749−3761.
(45) Gutov, O. V.; Gonzalez Hevia, M.; Escudero-Adan, E. C.; Shafir, A. Metal-Organic Framework (MOF) Defects under Control: Insights into the Missing Linker Sites and Their Implication in the Reactivity of Zirconium-Based Frameworks. *Inorg. Chem.* **2015**, *54*, 8396−8400.
(46) Taddei, M. When defects turn into virtues: The curious case of zirconium-based metal-organic frameworks. *Coord. Chem. Rev.* **2017**, *343*, 1−24.

DOI: 10.1021/acs.inorgchem.7b03063
Inorg. Chem. XXXX, XXX, XXX−XXX

(47) Klet, R. C.; Liu, Y.; Wang, T. C.; Hupp, J. T.; Farha, O. K. Evaluation of Brønsted acidity and proton topology in Zr- and Hf-based metal−organic frameworks using potentiometric acid−base titration. *J. Mater. Chem. A* **2016**, *4*, 1479−1485.
(48) Dixon, W. T.; Schaefer, J.; Sefcik, M. D.; Stejskal, E. O.; McKay, R. A. Total suppression of sidebands in CPMAS C-13 NMR. *J. Magn. Reson.* **1982**, *49*, 341−345.
(49) Vitaku, E.; Smith, D. T.; Njardarson, J. T. Analysis of the structural diversity, substitution patterns, and frequency of nitrogen heterocycles among U.S. FDA approved pharmaceuticals. *J. Med. Chem.* **2014**, *57*, 10257−10274.
(50) Horton, D. A.; Bourne, G. T.; Smythe, M. L. The combinatorial synthesis of bicyclic privileged structures or privileged substructures. *Chem. Rev.* **2003**, *103*, 893−930.
(51) Humphrey, G. R.; Kuethe, J. T. Practical methodologies for the synthesis of indoles. *Chem. Rev.* **2006**, *106*, 2875−2911.
(52) Yang, Z.; Xia, C.; Liu, D.; Liu, Y.; Sugiya, M.; Imamoto, T.; Zhang, W. P-stereogenic PNP pincer-Pd catalyzed intramolecular hydroamination of amino-1,3-dienes. *Org. Biomol. Chem.* **2015**, *13*, 2694−2702.
(53) Pierson, J. M.; Ingalls, E. L.; Vo, R. D.; Michael, F. E. Palladium(II)-catalyzed intramolecular hydroamination of 1,3-dienes to give homoallylic amines. *Angew. Chem., Int. Ed.* **2013**, *52*, 13311−13313.
(54) McGhee, A.; Cochran, B. M.; Stenmark, T. A.; Michael, F. E. Stereoselective synthesis of 2,5-disubstituted morpholines using a palladium-catalyzed hydroamination reaction. *Chem. Commun.* **2013**, *49*, 6800−6802.
(55) Cucciolito, M. E.; D'Amora, A.; Vitagliano, A. Catalytic Hydroalkylation of Olefins by Stabilized Carbon Nucleophiles Promoted by Dicationic Platinum(II) and Palladium(II) Complexes. *Organometallics* **2010**, *29*, 5878−5884.
(56) Cochran, B. M.; Michael, F. E. Synthesis of 2,6-disubstituted piperazines by a diastereoselective palladium-catalyzed hydroamination reaction. *Org. Lett.* **2008**, *10*, 329−332.
(57) Cochran, B. M.; Michael, F. E. Mechanistic studies of a palladium-catalyzed intramolecular hydroamination of unactivated alkenes: protonolysis of a stable palladium alkyl complex is the turnover-limiting step. *J. Am. Chem. Soc.* **2008**, *130*, 2786−2792.
(58) Michael, F. E.; Cochran, B. M. Room temperature palladium-catalyzed intramolecular hydroamination of unactivated alkenes. *J. Am. Chem. Soc.* **2006**, *128*, 4246−4247.
(59) Kawatsura, M.; Hartwig, J. F. Transition Metal-Catalyzed Addition of Amines to Acrylic Acid Derivatives. A High-Throughput Method for Evaluating Hydroamination of Primary and Secondary Alkylamines. *Organometallics* **2001**, *20*, 1960−1964.
(60) Aprile, A.; Iversen, K. J.; Wilson, D. J.; Dutton, J. L. Te(II)/Te(IV) Mediated C-N Bond Formation on 2,5-Diphenyltellurophene and a Reassignment of the Product from the Reaction of PhI(OAc)2 with 2 TMS-OTf. *Inorg. Chem.* **2015**, *54*, 4934−4939.
(61) Drew, D.; Doyle, J. R.; Shaver, A. G. Cyclic Diolefin Complexes of Platinum and Palladium. *Inorg. Synth.* **2007**, *13*, 47−55.
(62) Maaliki, C.; Chevalier, Y.; Thiery, E.; Thibonnet, J. Palladium and copper catalyzed Sonogashira decarboxylative coupling of aryl iodides and alkynyl carboxylic acids. *Tetrahedron Lett.* **2016**, *57*, 3358−3362.
(63) Smallcombe, S. H.; Patt, S. L.; Keifer, P. A. WET Solvent Suppression and Its Applications to LC NMR and High-Resolution NMR Spectroscopy. *J. Magn. Reson., Ser. A* **1995**, *117*, 295−303.

DOI: 10.1021/acs.inorgchem.7b03063
Inorg. Chem. XXXX, XXX, XXX−XXX